

# Space-time in motion: An evolving relativistic binary black hole metric for GIZMO

Giacomo Fedrigo<sup>1,2,\*</sup>, Alessandro Lupi<sup>1,2,3</sup>, Alessia Franchini<sup>2,4</sup>, and Matteo Bonetti<sup>2,5,6</sup>

<sup>1</sup> Como Lake centre for AstroPhysics, DiSAT, Università dell’Insubria, Via Valleggio 11, 22100 Como, Italy

<sup>2</sup> INFN, Sezione di Milano-Bicocca, Piazza della Scienza 3, I-20126 Milano, Italy

<sup>3</sup> INAF – Osservatorio di Astrofisica e Scienza dello Spazio di Bologna, Via Gobetti 93/3, I-40129 Bologna, Italy

<sup>4</sup> Dipartimento di Fisica “A. Pontremoli”, Università degli Studi di Milano, Via Giovanni Celoria 16, 20134 Milano, Italy

<sup>5</sup> Dipartimento di Fisica “G. Occhialini”, Università degli Studi di Milano-Bicocca, Piazza della Scienza 3, I-20126 Milano, Italy

<sup>6</sup> INAF – Osservatorio Astronomico di Brera, Via Brera 20, I-20121 Milano, Italy

Received 13 November 2025 / Accepted 26 February 2026

## ABSTRACT

The last evolutionary stages of massive black hole binaries prior to coalescence are dominated by the emission of gravitational waves, which will be probed by the future Laser Interferometer Space Antenna. If gas is present around the two black holes, the associated electromagnetic emission can provide additional information about the binary properties and location before the merger event. For this reason, a proper characterisation of the electromagnetic emission during these phases is of fundamental importance, and requires a detailed description of the gas dynamics close to the event horizon of the two black holes; this is only achievable via numerical simulations. Within this context, we present the implementation of the superposed Kerr-Schild dynamic metric in the relativistic scheme in the meshless code GIZMO. Our code can now simulate black hole binaries approaching a merger with high computational efficiency and accuracy, taking relativistic effects on the gas into account. To validate our implementation, we performed two tests. First, we explored the case of a relativistic Bondi flow around a binary, finding very good agreement with numerical relativity simulations. Then, we explored the case of an inviscid relativistic circumbinary disc, comparing our results with a similar simulation run assuming Newtonian gravity. In this second case, we find moderate differences in the mass accretion rate and in the inflow dynamics, which suggest that the presence of a non-Keplerian potential and apsidal precession in the orbiting gas trajectories produce stronger shocks and boost angular momentum transport in the disc. Our work highlights the importance of accounting for relativistic corrections in accretion disc simulations around black hole binaries approaching a merger, even at scales much larger than those currently probed by numerical relativity simulations.

**Key words.** accretion, accretion disks – black hole physics – hydrodynamics – plasmas – relativistic processes – methods: numerical

## 1. Introduction

In the next decade, the Laser Interferometer Space Antenna (LISA) mission is expected to detect gravitational wave (GW) signals in the millihertz regime emitted by massive black hole binaries (MBHBs) approaching a merger (Kocsis et al. 2006; Dotti et al. 2006; Mayer et al. 2007; Amaro-Seoane et al. 2012; Capelo et al. 2015; Amaro-Seoane et al. 2017). These sources reside in the centre of galaxies and are expected to evolve and eventually merge in gas-rich environments. The presence of gas and the highly dynamic space-time suggest the possibility of accretion onto the binary components, resulting in the production of strong electromagnetic (EM) signals. Therefore, MBHBs close to merging represent the perfect scenario for multi-messenger astronomy with massive compact objects. The coincident detection of a GW signal and an EM counterpart could provide unique information about the system’s environment and evolution.

Furthermore, the pulsar timing array (PTA) community recently announced the detection of a stochastic GW background signal in the nanohertz frequency band (EPTA Collaboration 2023; Agazie et al. 2023; Reardon et al. 2023; Xu et al. 2023), likely produced by a population of  $10^8$ – $10^9 M_{\odot}$  black hole (BH) binaries. These PTA results showcase our deep understanding of the GW signal produced by massive compact objects while

also providing a first proof of the existence of close-separation MBHBs.

Still, there is considerable uncertainty about the signature features of an EM signal produced by a MBHB that make the source distinguishable from a single active galactic nucleus (Bogdanović et al. 2011; Dotti et al. 2012; Bogdanović et al. 2022) and that cannot be explained by other mechanisms, for example asymmetric emissions or a periodic modulation of an active galactic nucleus disc (Rigamonti et al. 2025; Dotti et al. 2023). Major differences may exist in the accretion flows close to the central binary. The non-axisymmetric potential of a binary could carve an empty cavity around the BHs due to strong torques while thin streams of gas fall into the centre and are accreted by the compact objects (MacFadyen & Milosavljević 2008; Noble et al. 2012), yielding characteristic EM features. The dynamics of these processes may depend strongly on the spins of the BHs and on the properties of the gaseous environment (Bowen et al. 2018; Bode et al. 2010; Cattorini et al. 2021; Ruiz et al. 2023). Variability in the emitted light curves is also observed in many simulations (Krauth et al. 2023; Gutiérrez et al. 2022; Franchini et al. 2024a; Cocchiararo et al. 2024, 2025) and could be a smoking gun for detecting an evolving MBHB with optical facilities such as the Vera Rubin Observatory’s Large Synoptic Survey Telescope (LSST) (Chiesa et al. 2025).

Numerical simulations are powerful tools for studying and understanding such extreme environments and can help predict

\* Corresponding author: [gfedrigo@uninsubria.it](mailto:gfedrigo@uninsubria.it)

the EM emission from a MBHB approaching a merger. Many studies aim to reach a stationary regime to study the properties of a circumbinary disc. Therefore, starting from idealised initial conditions, it is necessary to simulate the system for hundreds of orbits, as discussed in the binary disc code comparison presented in [Duffell et al. \(2024\)](#). Hence, many studies have focused on long-term Newtonian simulations, both in 2D and in 3D ([Muñoz et al. 2020](#); [Krauth et al. 2023](#)), also considering post-Newtonian (PN) corrections to the binary evolution ([Franchini et al. 2024a](#)).

On the other hand, many interesting accretion features exclusive to a MBHB system may reside close to the event horizons ([d’Ascoli et al. 2018](#); [Gold 2019](#); [Cattorini & Giacomazzo 2024](#)). To accurately explore those regions, 3D numerical relativity simulations are necessary. However, these kinds of simulations are extremely computationally expensive and are therefore limited to evolving BH binaries only for a few orbits before the merger ([Bode et al. 2010](#); [Giacomazzo et al. 2012](#); [Gold et al. 2014](#); [Paschalidis et al. 2021](#); [Fedrigo et al. 2024](#)). Only recently have hybrid and approximated methods been employed to solve this issue and evolve the system for a longer time ([Mignon-Risse et al. 2023](#); [Avara et al. 2024](#); [Ennoggi et al. 2025a,b](#)).

A simpler solution is presented by [Combi et al. \(2021\)](#) and [Combi & Ressler \(2026\)](#) in the form of an approximated dynamic metric created by the superposition of two boosted BHs in Kerr-Schild (KS) coordinates, called the superposed Kerr-Schild (SKS) metric. It represents an accurate yet computationally cheap way to evaluate the dynamic metric of a BH binary, and it can be used to perform general relativistic magnetohydrodynamic (GRMHD) or ray-tracing simulations. Thanks to the high versatility of the SKS metric, it is now possible to explore in depth the evolution and dynamics of the gaseous environment in which MBHBs reside using different state-of-the-art astrophysical codes.

In this work we present the implementation of the SKS metric in the relativistic meshless version of the GIZMO code ([Hopkins 2015](#); [Lupi 2023](#); [Fedrigo & Lupi 2025](#)). Our goal is to build a code that can evolve relativistic circumbinary discs around BH binaries for thousands of orbits, to study their properties and search for unique signatures.

In Sect. 2.1 we briefly review the SKS formulation, and in Sect. 2.2 we present some details regarding its implementation in GIZMO. Then, in Sect. 3, we report results from two tests we performed to verify the metric was correctly implemented and verify its stability within the code. The first test compared our results with a numerical relativity simulation of a uniform gas distribution accreting onto a BH binary (Sect. 3.1). With the second test, we explored the differences between a Newtonian and a relativistic circumbinary disc (Sect. 3.2). Finally, we draw our conclusions in Sect. 4.

## 2. Black hole binary metric

In this section we describe the implementation of the SKS metric in GIZMO. The relativistic scheme implemented in GIZMO is presented in [Lupi \(2023, hydrodynamics\)](#) and [Fedrigo & Lupi \(2025, magnetohydrodynamics\)](#). Note that we do not consider magnetic fields in the tests discussed in this work, deferring the analysis of magnetised plasma in a MBHB environment to a future study. The superposed binary metric was first introduced in [Lopez Armengol et al. \(2021\)](#), later refined in [Combi et al. \(2021\)](#), and finally extended to include the merger phase in [Combi & Ressler \(2026, hereafter Co24\)](#). Here, we

briefly review the main concepts of the Co24 metric formulation, and we then focus on some implementation details. Throughout this work, we employ natural units, i.e.  $G = c = 1$ .

### 2.1. SKS formulation

The metric of a single spinning BH of mass  $M$  and spin  $\mathbf{a}$  can be expressed in the ‘Cartesian’ KS coordinate system  $\{X^\mu\}$ :

$$g_{\mu\nu} = \eta_{\mu\nu} + 2\mathcal{H}l_\mu l_\nu, \quad (1)$$

where the null vector  $l$  is defined by

$$l_\mu dX^\mu = dt + \frac{1}{r^2 + a^2} \left[ rX^i - \epsilon_{jk}^i a^j X^k + \frac{a^i X^j \delta_{ij}}{r} a^i \right] dX_i, \quad (2)$$

the function  $\mathcal{H}$  is

$$\mathcal{H}(X^i) = \frac{Mr^3}{r^4 + (a^i X^j \delta_{ij})^2}, \quad (3)$$

the Boyer-Lindquist radius is

$$r = \sqrt{\frac{R^2 - a^2 + \sqrt{(R^2 - a^2)^2 + 4(a^i X^j \delta_{ij})^2}}{2}}, \quad (4)$$

and  $R^2 = X^2 + Y^2 + Z^2$ .

Following Co24, a generalised Lorentz boost transformation is then applied to the KS metric (Eq. 1), going from the non-inertial frame at rest with the BH  $\{X^\mu\}$  to an inertial frame where the BH is moving on an inspiralling orbit,  $\{x^\mu\}$ . Defining the BH trajectory with  $\mathbf{s}(t)$ , the coordinate transformation with velocity  $\mathbf{v} = \beta\mathbf{n}(t)$  is given by

$$\begin{aligned} T &= t - W\beta(n_x\bar{x} + n_y\bar{y} + n_z\bar{z}), \\ X &= \bar{x}[1 + n_x^2(W-1)] + \bar{y}(W-1)n_x n_y + \bar{z}(W-1)n_x n_z, \\ Y &= \bar{y}[1 + n_y^2(W-1)] + \bar{x}(W-1)n_x n_y + \bar{z}(W-1)n_y n_z, \\ Z &= \bar{z}[1 + n_z^2(W-1)] + \bar{y}(W-1)n_y n_z + \bar{x}(W-1)n_x n_z, \end{aligned} \quad (5)$$

where  $\bar{x}^i = x^i - s^i(t)$  and  $W$  is the Lorentz factor. To conclude, the superposed metric of two inspiralling spinning BHs in KS coordinates can be written as

$$g_{\mu\nu} = \eta_{\mu\nu} + \left[ 2 \frac{\partial X^\rho}{\partial x^\mu} \frac{\partial X^\sigma}{\partial x^\nu} \mathcal{H} l_\rho l_\sigma \right]_1 + \left[ 2 \frac{\partial X^\rho}{\partial x^\mu} \frac{\partial X^\sigma}{\partial x^\nu} \mathcal{H} l_\rho l_\sigma \right]_2. \quad (6)$$

This approximate metric formulation exhibits good accuracy and low constraint violation for intermediate binary separations, but it begins to fail at BH separations  $\lesssim 8M$ . The SKS metric performs well and is smooth at the innermost stable circular orbit regions, which are important features to take into consideration in order to correctly evolve the accretion disc dynamics (see the space-time analysis in [Combi et al. 2021](#)). While the Co24 metric formulation also encompasses the merger phase, we did not take this feature into consideration in this work, with the exception of the Bondi-like test in which we evolved the binary until the merger moment (Sect. 3.1).

### 2.2. SKS implementation in GIZMO

The SKS formulation, as presented in Co24, has been coded in a public, ready-to-use C implementation ([Combi & Ressler 2024](#)) that takes the BH parameters as input data and returns the covariant metric from Eq. (6) at a given position. At each timestep, the

needed inputs are the positions, velocities, spins, and masses of each BH. In our implementation, we took advantage of the BH particle structure already present in the Newtonian version of the code (see Franchini et al. 2022, 2023, 2024a), from which we exported the BH parameters. Hence, the binary is described by two BH particles that are evolved live, and their properties can be influenced by the interaction with the surrounding gas. Simulations presented in Franchini et al. (2023) show the importance of evolving live binaries, highlighting crucial differences in the conservation of the total angular momentum of the system, in the binary separation evolution, and in the effects of gravitational torques. In this work, however, we neglected the change in BH masses and spin driven by the gaseous disc for simplicity. This choice is reasonable as we assumed our discs to have much lower masses compared with the binary and therefore to have a negligible effect on its dynamical evolution. The focus here is instead to investigate the changes that the general relativity treatment brings to the gas dynamics.

We integrate the equation of motion considering PN corrections up to the 2.5 PN order, i.e. including the contribution of the GW emission to the orbital evolution (Blanchet 2014), to evaluate the BH trajectories. We refer to Franchini et al. (2024a) for a complete presentation of the PN implementation in GIZMO<sup>1</sup>.

During the system evolution, gas can be accreted by the BHs. In our implementation, at each timestep, the code evaluates the distance of each gas particle to both BHs and identifies the closest one. When such a distance becomes smaller than a user-defined excision radius, the gas particle is removed from the simulation. Since the superposed metric is written in the horizon-penetrating KS coordinate system, we usually set the excision radius to reside inside the event horizon. As mentioned above, in this work we did not change the BH properties when gas particles are accreted onto the horizons. This represents a sufficiently good approximation if  $M_{\text{BH}} \gg M_{\text{gas}}$ , as we assumed in our work. To keep track of the accretion onto the BH during the simulation, at each timestep we also store the properties of the particles crossing the closest BH's event horizon radius.

We used the on-the-fly adaptive particle splitting approach, as presented in Franchini et al. (2022). With this procedure, particles are split according to a scheme that depends on the particle distance to the domain centre. In practice, the mass resolution is doubled each time the gas crosses a set of defined radii, to better resolve the disc edge and the accretion streams inside the inner disc cavity. We refer to Franchini et al. (2022) for an in-depth presentation of this refinement approach. The only difference with the relativistic version is that, in the latter, while the two child particles inherit the hydrodynamic properties of the parent one, the metric coefficients are recomputed at the location of the two new particles.

Finally, when the resolution is poor, gas particles close to the BH's event horizon might cause the neighbour search to be extended to particles located on the other side of the BH. Such a case would either produce spurious results (as the gas cells should be causally disconnected from each other) or, in the worst-case scenario, completely break the code. To avoid such events in our algorithm, the neighbour search in our implementation is limited to a maximum distance equal to the current distance of the particle from the closest BH. Note that we performed accretion tests while varying the excision radius and with different neighbour search prescriptions, for example letting the kernel extend over the BH but preventing particle pairs whose line of sight is directly obscured by a BH from interacting. All the tests yielded comparable results, without any statistically significant differences.

<sup>1</sup> Note that the code can also work with pre-computed trajectories such as those provided by the CBWAVES tool (Csizmadia et al. 2012).

### 3. Metric validation tests

In this section we present the two general relativistic (GR) hydrodynamic tests we performed to confirm the correct implementation of the SKS metric in our code<sup>2</sup>. We studied a set of inspiralling binaries at close and intermediate separations, surrounded by two different gaseous environments: a uniform plasma distribution and a thin circumbinary disc. We compared our results with those obtained using different evolution schemes. We focused on a comparison of the gas distribution and the mass accretion rate onto the horizons.

#### 3.1. Bondi accretion

As a first test, we evolved an equal-mass binary initially placed on a circular orbit with a separation of  $12M$ . For simplicity, in this test we did not include any live BH particle, but we defined the BH location through pre-computed trajectories using CBWAVES, which included PN corrections up to order 3.5. We embedded the binary in a homogeneous gas distribution initially at rest extending up to  $1500M$  and let the system evolve towards a Bondi-like solution around the binary system, similarly to the un-magnetised case studied by Cattorini et al. (2021). Having such a large domain is important as we want the simulation to last for several orbits without including any particle injection at the outer boundary. At the same time, sampling the gas distribution with enough resolution to properly resolve the event horizon with several gas cells is crucial, as preliminary tests at low resolution showed spurious density fluctuations at the centre of the domain when the number of cells was too low.

Fulfilling both requirements at the same time would require an extremely high number of particles, which would make the simulation unfeasible. To overcome this limitation, we decided to include adaptive particle splitting during the simulation, which operates between  $50M$  and  $1000M$ , increasing the resolution by a factor of  $2^{10}$  following a parabolic splitting function (see Franchini et al. 2022 for details). Moreover, we also mapped the initial conditions using the same splitting function employed during the simulation, which resulted in 20 million particles with variable masses, instead of the tens of billions of particles required with a constant mass resolution everywhere. As we neglected the contribution of the gas self-gravity (see Franchini et al. 2021, 2024b for discs with self-gravity), the particle splitting does not introduce any spurious effect in the calculations while guaranteeing a very high resolution close to the binary from the beginning. To prevent particles at the outer edge from leaving the domain, we further constrained the location and the hydrodynamic properties of the outermost five particle spherical shells to remain constant over time.

For this specific test, we evolved the system for the last 5 hours before the merger, which occurs at  $t = 1772$  for a binary with  $M = 10^6 M_{\odot}$ , assuming an ideal gas law with  $\Gamma = 4/3$ . In Fig. 1 we show the accretion rate onto each BH measured during the simulation, compared with the numerical relativity simulation results from Cattorini et al. (2021). Given the symmetry of the system, the accretion rates onto the BHs are exactly the same, as expected. After an initial rise, the accretion rate reaches a plateau that corresponds to the Bondi-like solution, in agreement with the results from Cattorini et al. (2021). At later times, both simulations exhibit an increasing accretion rate as the two

<sup>2</sup> As an internal-consistency check, we also verified that the SKS metric recovers the single Kerr metric when one of the two BH masses is set to zero and the massive BH is set to rest, by integrating circular orbits of collisionless particles.

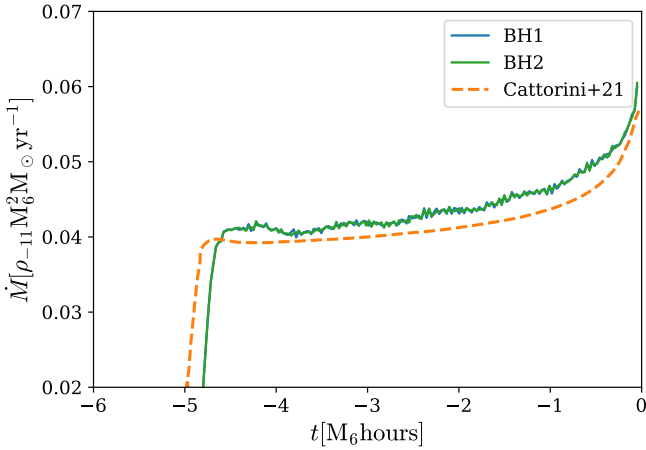


**Fig. 1.** Mass accretion rate as a function of time in the Bondi-like test. The solution from Cattorini et al. (2021) is shown with the orange line.

BHs approach the merger. Compared with the numerical relativity results, the approximated metric slightly overestimates the gravitational pull onto the BHs, which results in a roughly 10 percent higher accretion rate (Combi & Ressler 2026). Considering (i) the different space-time evolution in the two cases, (ii) differences in the numerical techniques employed and the discretisation scheme, and (iii) the maximum resolution close to the horizon, which in our case is about  $0.4M$ , much lower than the resolution reached by Cattorini et al. (2021), i.e.  $0.02M$ , these differences do not appear particularly significant, especially when we consider that our simulation required only 40 hours on 48 CPUs. Note also that in numerical relativity simulations, the space-time perturbations due to the two BHs close to merging are expected to differ from the analytic metric from Co24, potentially causing inaccuracies in the accretion rate calculation as well. Moreover, the accretion rates in grid-based simulations are typically estimated by integrating the mass flux at the horizon surface, whereas in GIZMO we can directly tag the particles crossing it. We can therefore conclude that our treatment of the binary dynamics is sufficiently robust, and we can proceed by running simulations of binaries embedded in circumbinary discs.

### 3.2. Circumbinary disc evolution

We directly compared a circumbinary disc evolved with the Newtonian version of GIZMO with one evolved with our GR implementation in order to study the effects of the SKS metric implementation on the gas evolution. For both runs, we considered the same initial conditions, which correspond to those used in Franchini et al. (2022, 2023) and produced with the code PHANTOM (Price et al. 2017). We initialised  $10^6$  particles, sampling a Newtonian accretion disc extending from  $R_{\text{in}} = 150M$  to  $R_{\text{out}} = 1000M$ . The initial aspect ratio,  $H/R$ , was 0.1. The BH binary was initialised on a circular orbit with a separation  $d = 100M$ , and the BHs were non-spinning. We note that the initial configuration was fully Newtonian. This assumption is well justified because the initial binary separation was sufficiently large and the disc was far enough from the BHs to ensure that relativistic corrections played only a minor role. As an equation of state, we used the ideal gas relation, with  $\Gamma = 5/3$ , both in the initial conditions and during the evolution.

We performed the first run using the Newtonian version of the code, where the gas is evolved according to the classical

hydrodynamic equation and the binary potential is given by the superposition of the two Keplerian potentials generated by the BH particles. The second run was evolved with the GR scheme, where the gas follows the equations of GR hydrodynamics as presented in Lupi (2023) and with the improvements described in Fedrigo & Lupi (2025), evaluated on the SKS metric. In both cases, we employed the meshless finite-volume (MFM) method and adaptive particle splitting (Franchini et al. 2022), and the BH dynamics was evaluated considering PN correction terms up to the 2.5 order. For simplicity, we decided to evolve both discs as inviscid, thus without either viscosity or magnetic field prescriptions (the latter will be the focus of an upcoming work). Although idealised, this test allowed us to focus solely on the relativistic effects of the binary metric on the gas, without any additional processes that might affect the comparison. The angular momentum transport therefore occurs only via asymmetries in the flow and possible numerical dissipation.

A more comprehensive description of the physics within accretion discs would require solving the radiative transport equations during the hydrodynamic evolution of the system, which would possibly affect the thermodynamics and the structure of the disc (Kaaz et al. 2025). However, such a prescription would be computationally very demanding. A much simpler approach would be to artificially cool the gas to a target entropy, as done in Noble et al. (2012) and Combi et al. (2022), where the evolved discs appeared thinner and with less vertical pressure support (d’Ascoli et al. 2018). In our simulations, however, we decided to neglect any gas cooling prescription to keep the problem as simple as possible. As a consequence, we expected our discs to become warmer and thicker over time. We let the two systems evolve until  $t = 200T_0$ , where  $T_0$  is the orbital period of the binary at  $t = 0$ .

In Fig. 2 we show density maps of the two evolved circumbinary discs at  $t = 200T_0$ . In the Newtonian snapshot (right panel), an empty, slightly elliptical cavity is formed around the binary, carved by the torques produced by the orbiting BHs. The edge of the cavity is found at approximately  $r \approx 200\text{--}250M$ , i.e.  $\sim 2d$ , consistent with previous simulations. A faint gas stream can be seen accreting from the disc onto the horizon of one of the BHs.

On the other hand, in the GR evolution (left panel), there is a slightly smaller and more circular internal cavity and a lower density in the inner region of the disc. The inner cavity extends up to  $r \approx 150\text{--}200M$ , while a second under-dense region can be seen extending up to  $r \approx 500M$ . As expected, both discs become thicker over time, reaching  $H/R$  ratios of  $\sim 0.15$ .

At late times, after  $\approx 100$  orbital periods, both discs appear asymmetric, with a  $m = 1$  weak overdensity, which is usually referred to as ‘lump’ (Shi et al. 2012; Noble et al. 2012; Mignon-Risse et al. 2023). This feature is believed to be caused by streams of gas falling into the central cavity and redirected outwards towards the inner edge of the circumbinary disc, and it is observed in both magnetised and non-magnetised circumbinary discs (Noble et al. 2021) around either equal-mass or unequal-mass binaries, provided that the mass ratio is high enough. The gas accumulates in a region that is usually a few times denser than the rest of the inner disc. The origin of the lump is often associated with the Rossby-wave instability (RWI), which can occur in the innermost regions of the circumbinary disc (Mignon-Risse et al. 2023). The RWI is expected to develop in the presence of local maxima in the fluid vortensity (Lovell et al. 1999). A simpler criterion for the development of the RWI requires the minima of epicyclic frequency ( $\kappa$ ) to be  $\min(\kappa^2) \lesssim 0.5\text{--}0.6\Omega^2$  (Chang & Youdin 2024). This condition can be satisfied in the presence of strong density gradients, such as the one between the cavity and the inner edge of the circumbinary disc.

We computed the ratio  $\kappa^2/\Omega^2$  within our circumbinary disc, finding values of  $\sim 0.5$  in the innermost regions, with smaller val-

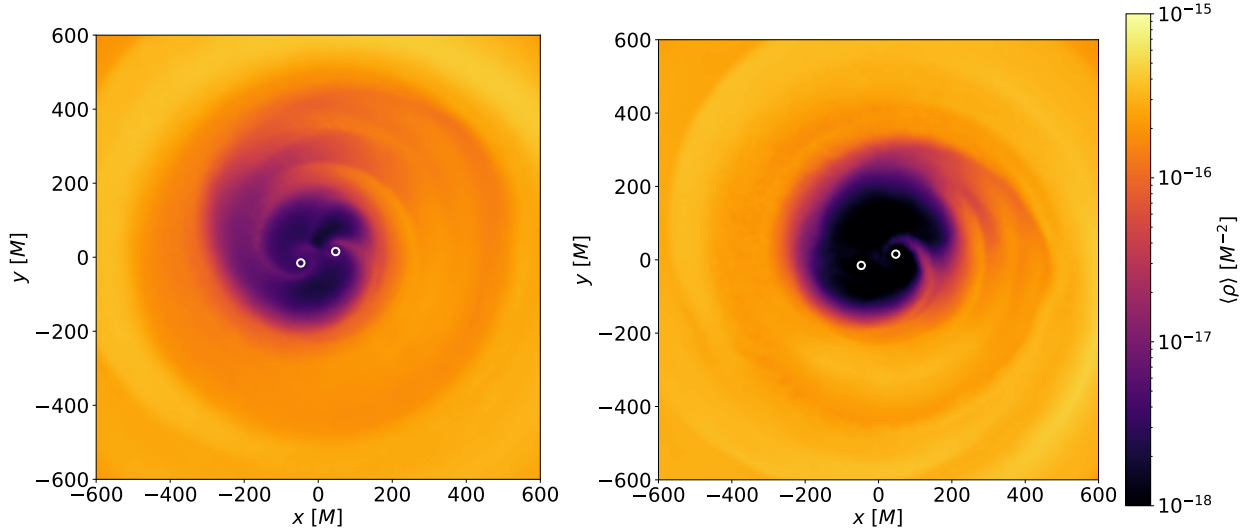


**Fig. 2.** Density map of the central part of the circumbinary disc for the GR run (left) and the Newtonian run (right), at  $t = 200T_0$ . Density is volume-averaged along the  $z$  direction. The white circles mark the BHs' event horizons, scaled up by a factor of 10 for visualisation purposes.

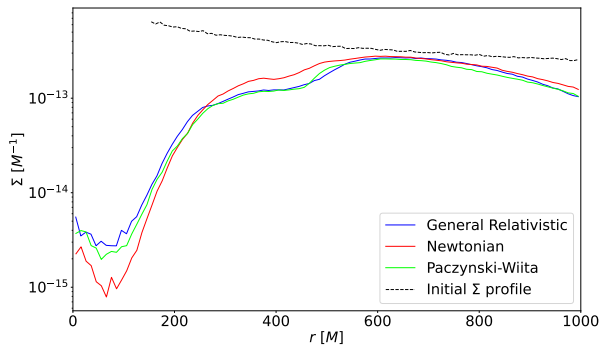


**Fig. 3.** Surface density ( $\Sigma$ ) radial profile for the GR (blue), Newtonian (red), and PW (lime) runs at  $t = 200T_0$ . The initial  $\Sigma$  profile is shown with a dashed black line.

ues limited to a very narrow radial range and only in our GR run. Our density gradient at the cavity edge does not seem strong enough to develop RWI, i.e. we find a ‘lump’ with a density contrast well within a factor of 2. The reason for such a weak ‘lump’ likely lies in the choice of the equation of state, i.e. adiabatic without cooling, and the dimensionality of the problem. For instance, prominent lumps have been found in circumbinary disc simulations that employ an isothermal fluid (Shi et al. 2012) or cooling prescriptions that efficiently dissipate extra heating from shocks (Noble et al. 2012). In the adiabatic case, a prominent lump is found in 2D simulations, which prevents the gas from redistributing along the  $z$  direction, boosting density gradients and, as a consequence, more easily triggering the RWI (Mignon-Risse et al. 2023).

For a more quantitative analysis, in Fig. 3 we plot the surface density ( $\Sigma$ ) radial profile for both runs at  $t = 200T_0$ . In the innermost region, the Newtonian evolution yields a surface density that is 2–3 times higher than in the GR case, indicating that less gas is entering the central cavity. Between  $r \approx 250M$  and  $r \approx 500M$ , a small drop in the  $\Sigma$  profile highlights the underdense region discussed above. This feature is more pronounced in the relativistic run, with a drop by a factor of 2. We elaborate on this discrepancy further below in this section.

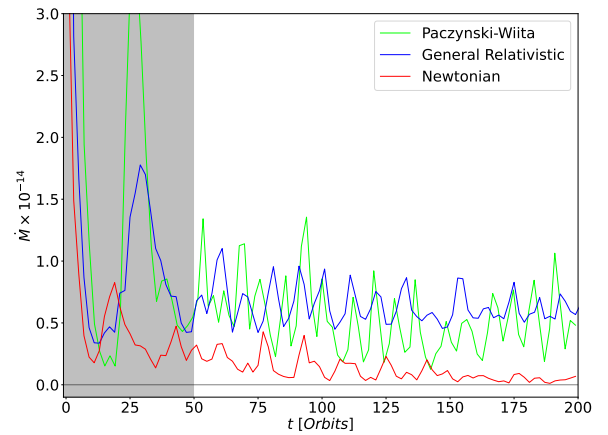


**Fig. 4.** Mass accretion rate as a function of time for the GR (blue), Newtonian (red), and PW (lime) binaries. The transient phase, caused by the initial data relaxation, is marked with grey shading.

Finally, we evaluated the total mass accretion rate onto the BHs' event horizons ( $\dot{M}$ ) and show it in Fig. 4. As expected, after an initial transient (grey shaded region), the Newtonian binary (red line) exhibits low gas accretion, with a slow decay over time. We recall that there is no viscosity or magnetic field prescription in the simulations, which are usually the principal processes invoked to transport angular momentum and promote accretion. We note that the adaptive particle splitting procedure can introduce a small diffusivity in the evolution scheme at the radii where the resolution is refined<sup>3</sup>. However, its adoption in our work enabled us to better resolve the gas morphology within the cavity (Franchini et al. 2022; Duffell et al. 2024). We opted to use the adaptive resolution to correctly resolve the internal structure at the cost of introducing a small diffusivity.

The GR binary (blue line in Fig. 4) shows a non-zero accretion rate characterised by a constant average trend and a quasi-periodic variability related to the inner disc orbital motion. These

<sup>3</sup> During the testing, we found that the splitting procedure in the GR scheme is slightly more diffusive than the Newtonian one. However, in our runs, this difference results in a  $\dot{M}$  increase of  $10^{-2} \langle \dot{M} \rangle$ .

kinds of oscillations have been seen and studied in depth in many other studies (Paschalidis et al. 2021; Combi et al. 2022; Cattorini et al. 2022; Bright & Paschalidis 2023; Fedrigo et al. 2024; Manikantan et al. 2025). We note that the presence of a non-zero accretion rate in the GR run is consistent with the density drop found in the  $\Sigma$  profile between  $r \approx 200$  and  $500M$  (Fig. 3). The accreting gas comes from this inner part of the disc, which becomes less dense over time<sup>4</sup>.

Given the differences between the Newtonian and GR numerical schemes, such a difference might arise due to multiple factors, both numerical or physical. For this reason, we performed tests using more diffusive slope limiters in the Newtonian binary evolution, which resulted in a slightly higher mass accretion rate compared with the reference case. However, even with a higher numerical diffusion, the Newtonian accretion rate remains lower than in the GR run, suggesting that the diffusivity of the scheme cannot explain the different inflow onto the binary in the two cases<sup>5</sup>.

### 3.2.1. Post-Newtonian validation test

A physical explanation would be that the higher gas accretion rate is instead due to the non-Keplerian nature of the potential. To test this hypothesis, we performed a run using the Paczynski-Wiita (PW) potential implemented in the Newtonian scheme. The PW potential for a binary can be written as

$$\Phi(\mathbf{x}) = -\frac{GM_1}{(|\mathbf{x} - \mathbf{x}_1| - r_1^{\text{EH}})} - \frac{GM_2}{(|\mathbf{x} - \mathbf{x}_2| - r_2^{\text{EH}})}, \quad (7)$$

where  $|\mathbf{x} - \mathbf{x}_i|$  is the distance between the point where the potential is evaluated and the  $i$ -th BH, and  $r_i^{\text{EH}}$  is the radius of the  $i$ -th BH's event horizon. This PN potential (Paczynski & Wiita 1980) only produces two-thirds of the apsidal precession produced by a relativistic Schwarzschild potential (in the single central object scenario), but it is extremely easy to implement and fast to compute. For this test, we started from the same initial conditions employed in the other two runs and let the system evolve for  $\sim 200$  orbits. The resulting  $\Sigma$  profile is shown in Fig. 3, and the  $\dot{M}$  in Fig. 4. We clearly see that the surface density profile in the PN run is very similar to the GR case. After the usual initial transient, the mass accretion rate displays a trend comparable with the GR case, with stronger oscillation but similar averaged values. In fact, the average  $\dot{M}$  computed between 50 and 200 orbits is  $\langle \dot{M} \rangle = 5.4 \cdot 10^{-15}$  for the PW run, while it amounts to  $6.4 \cdot 10^{-15}$  and  $1.2 \cdot 10^{-15}$  in the GR and Newtonian runs, respectively.

We suggest that relativistic apsidal precession of the gas orbiting a BH binary may play a significant role in the circumbinary disc scenario (Hénon 1965; Paczynski 1977; Rudak & Paczynski 1981). When the trajectories of the orbiting gas are forced by apsidal precession to cross, shocks are generated. During shocks, part of the kinetic energy is converted into thermal energy and angular momentum is transferred outwards, resulting in a net gas inflow towards the centre. To substantiate this idea, we show the density-weighted gas temperature distribution at  $t = 200T_0$  in Fig. 5, obtained by measuring the pressure and density from the simulation and then using  $P = \rho k_b T / m_p \mu$ . As expected, the GR disc tends to be about a factor of 2–3 hotter than its Newtonian equivalent in the region affected by shocks, in agreement with our

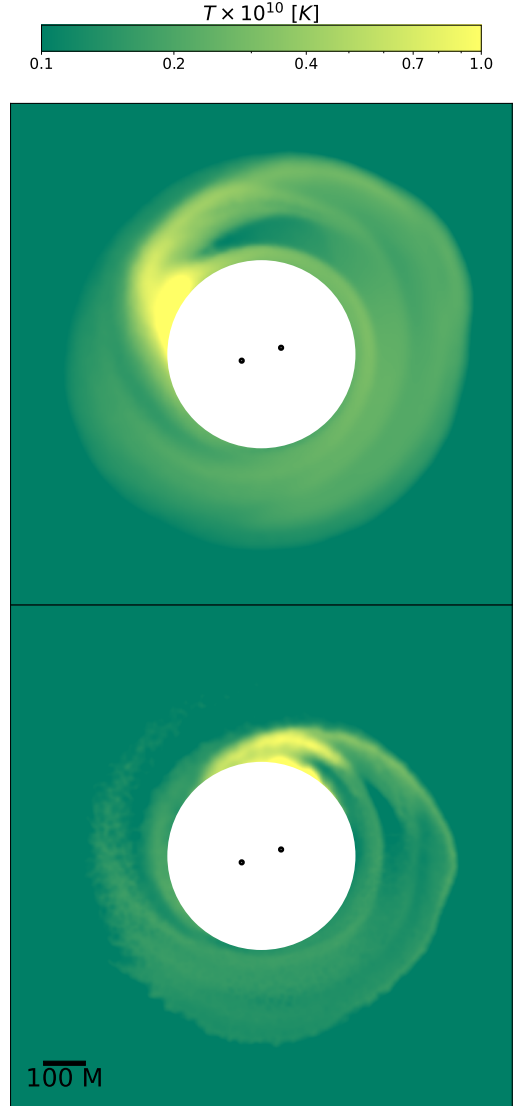


**Fig. 5.** Density-weighted gas temperature distribution at  $t = 200T_0$  for the GR (top) and Newtonian (bottom) runs. The inner cavity ( $r \lesssim 225M$ ) is masked with a white patch. The temperature is normalised for a binary of  $M_b = 10^6 M_\odot$ .

hypothesis. We also note that due to relativistic apsidal precession, the hottest area found at the inner edge of the relativistic disc is shifted forwards in the direction of the disc rotation relative to the Newtonian case. A gas cooling prescription could have mitigated this heating process in both our runs.

The presence of apsidal precession can therefore explain the higher mass accretion rate found in our GR and PW disc runs when compared with the Newtonian simulation. Even though this effect only slightly perturbs the gas trajectory, it can be enough to trigger a faint but non-negligible accretion process. Note that when a more realistic scenario is considered, for example including the presence of an effective viscosity or magnetic fields triggering magneto-rotational instability, the inflow rate we observed will likely be subdominant, thus going unnoticed in the presence of more efficient accretion mechanisms.

### 3.2.2. Angular momentum transport and effective viscosity

To measure the angular momentum transport within the disc, we computed the effective viscosity ( $\alpha_{\text{eff}}$ ) in our discs in different

<sup>4</sup> We let the relativistic run evolve until  $t = 600T_0$ ; a larger cavity with radius  $r \approx 500M$  is carved around the BHs.

<sup>5</sup> We also tested whether the initial conditions had any effect on the late-time dynamics of the gas in the disc, finding none.

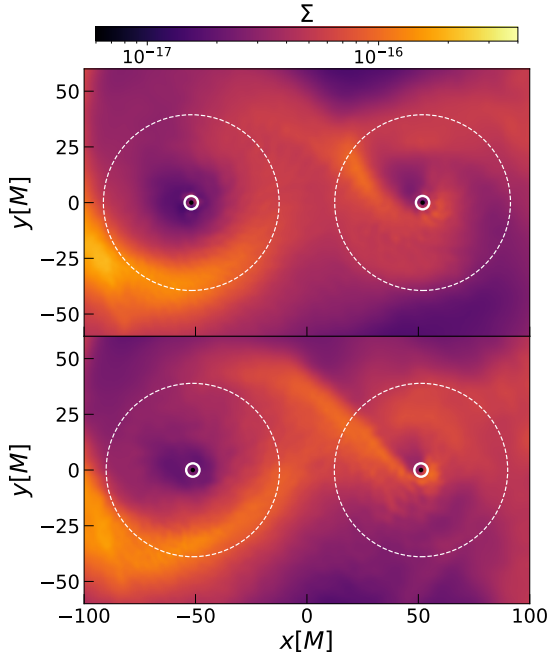


**Fig. 6.** Density maps of the minidisks during a filling phase (after  $\approx 60$  BH orbits from the start of the run) for the GR (top) and Newtonian (bottom) runs. The black dots mark the event horizons, the solid lines the innermost stable circular orbit radii, and the dashed lines the Roche lobe radii. Snapshots are aligned with the binary axis.

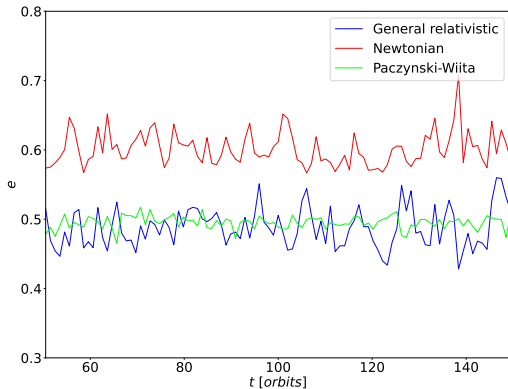


**Fig. 7.** Average gas eccentricity within the minidisks as a function of time for the GR (blue), Newtonian (red), and PW (lime) runs.

ways. First, we assumed the prescription by [Shakura & Sunyaev \(1973\)](#), who modelled the viscous stress tensor as simply proportional to the pressure in the disc,  $\alpha$  being the constant of proportionality. From this follows the expression for kinematic viscosity,  $\nu \equiv \alpha_{\text{eff}} c_s H$ . For a disc in a steady state, the kinematic viscosity is related to the mass accretion rate onto the central object and the disc surface density as  $\nu = \dot{M}/3\pi\Sigma$ . We computed the accretion rate radial profile within the disc by measuring the inward flux of material through cylindrical surfaces at different radii. We averaged the results over the last ten binary orbits, and we obtained values of  $\alpha_{\text{eff}}$  ranging between  $10^{-3}$  and  $10^{-2}$ . The values of the GR run are 3–5 times higher than the Newtonian one. We note that this quantity estimates the global angular momentum transport, taking the contributions from both hydrodynamic stresses and numerical dissipation into account.

Secondly, we computed the effective viscosity using its definition  $\langle R^r_\phi \rangle = \alpha_{\text{eff}} \langle P \rangle$ , where  $\langle R^r_\phi \rangle = \langle \rho h \delta u^r \delta u_\phi \rangle$  is the

Reynolds stress tensor,  $\delta u^\mu = u^\mu - \langle \rho u^\mu \rangle / \langle \rho \rangle$  is the velocity fluctuation relative to the mean motion, and  $\langle \cdot \rangle$  is a time and azimuthal average operator. We used the relativistic formalism presented in [Noble et al. \(2012\)](#), and we averaged again over the last ten binary orbits. Using this prescription, we obtained effective viscosity values of up to  $5 \times 10^{-3}$  and  $2 \times 10^{-3}$  in the outermost part of both discs for the GR and Newtonian run, respectively. A somewhat irregular behaviour is instead seen in the inner part of the disc, between  $r \approx 2.5d$  and  $r \approx 5d$ , where the development of spiral waves and asymmetries in the gas distribution results in a noisier local effective viscosity, with values reaching  $10^{-2}$  ([Mignon-Risse et al. 2025](#)). At the cavity edge,  $\alpha_{\text{eff}}$  reaches a maximum value of  $\sim 2.5 \times 10^{-2}$ . As suggested in [Noble et al. \(2012\)](#), we also computed the Reynolds stress tensor as  $\langle R^r_\phi \rangle = \langle T^r_\phi \rangle - \langle A^r_\phi \rangle$ , where  $T$  is the stress-energy tensor,  $\langle A^r_\phi \rangle = \langle \rho l \langle \rho h u^r \rangle \rangle / \langle \rho \rangle$ , and  $l = -u_\phi / u_t$  is specific angular momentum. As expected, this equivalent formulation yielded results compatible with the  $\alpha_{\text{eff}}$  estimation via the fluid velocity fluctuations.

Comparing the different  $\alpha_{\text{eff}}$  estimations, we can conclude that the angular momentum transport in our discs is dominated by the hydrodynamic stresses from fluid asymmetries. However, this effect yields an effective viscosity 1–2 orders of magnitude lower than values usually adopted in viscous disc simulations, for example  $\alpha \sim 0.1$  ([Franchini et al. 2024a](#)).

### 3.2.3. Minidisc morphology and dynamics

As a final analysis, we considered the morphology of the accreting structures that form close to the BHs’ horizons, usually called ‘minidisks’, which are expected to be affected by relativistic corrections. To define these structures, we considered the gas present within each BH’s Roche lobe ([Eggleton 1983](#)). In the case of an equal-mass binary, this region can be approximated as a sphere centred on the BH, with an equivalent-volume radius of  $R_{\text{eq}} \approx 0.38d$  ([Leahy & Leahy 2015](#)). We note that the very low angular momentum transport and the consequently low density in the central cavity lead to transient and highly variable ‘minidisc’ structures (Fig. 6) that are hardly comparable in morphology to those found in simulations with stronger angular momentum transport (e.g. GRMHD simulations in [Noble et al. 2012](#); [Combi et al. 2022](#) or viscous simulations in [Franchini et al. 2022](#)). However, they serve our purpose to study GR effects caused by the metric.

We compared the time evolution of minidisks in the two runs, finding a more uniform and homogeneous gas distribution in the relativistic case, and a more asymmetric distribution in the Newtonian one. Furthermore, the latter is more prone to strong density fluctuations, indicating moments where the Roche lobes are almost empty. The more stable evolution and the more homogeneous gas distribution of the GR minidisks can be understood in terms of the higher accretion rate in the cavity. Relativistic apsidal precession plays an important role here too. In our simulation, the gas streams falling towards the relativistic BHs circularise, producing more homogeneous gas structures around the BHs and effectively mitigating density asymmetries in the minidisks.

We evaluated the minidisc eccentricity in our simulations from the gas energy within the Roche lobes. We performed this analysis between  $t = 50T_0$  and  $t = 150T_0$ , i.e. excluding the initial transient and the final part of the simulations in which the Newtonian cavity is the emptiest, and we plot the results in Fig. 7. While the Newtonian minidisks show an eccentricity that oscillates around  $e \approx 0.6$ , the GR and PW ones average approximately to  $e \approx 0.5$ . Hence, the relativistic minidisks tend to be slightly more circular than the Newtonian ones. We note

that the circularisation effect is small because we are considering non-spinning BHs, whose apsidal precession effect is less strong when compared with spinning BHs.

Finally, we note that, while the PW prescription can produce results similar to our GR formulation in the scenario we considered here, it cannot emulate the spin of the BH and its effects on the gas dynamics. Also, the PW potential is divergent at the event horizon, which can lead to numerical instabilities and artefacts.

To conclude, our results highlight the importance of considering GR effects in the evolution of circumbinary discs and BHs' minidisks, as they play an important role even at distances as large as hundreds of gravitational radii and thousands of orbits before the binary merger.

## 4. Conclusions

In this paper we have presented our implementation of the SKS metric from Co24 in the relativistic scheme of the GIZMO code. The code can now simulate BH binaries at intermediate separations ( $10^1 M \lesssim d \lesssim 10^3 M$ ) with great computational efficiency and accuracy, taking relativistic effects in the gas and magnetic field evolution into account.

We tested our implementation by comparing our results with a numerical relativity simulation of a BH binary embedded in a uniform gas distribution, obtaining good agreement in the gas evolution behaviour and in the estimated mass accretion rate onto the BH horizons. Then, we compared the evolution of two circumbinary discs evolved using the Newtonian and relativistic schemes in GIZMO. Both simulations were stable and produced reasonable results. The GR run, however, yielded a higher rate of gas accreted onto the horizons and a lower-density region in the innermost part of the disc, between  $r \approx 2.5d$  and  $r \approx 5d$ . We find that the presence of a non-Keplerian potential is the cause of this phenomenon, as demonstrated by a PN simulation performed with the standard version of GIZMO.

With this work, we highlight the importance of including relativistic effects in simulations of circumbinary discs around BH binaries approaching a merger, even at scales not yet accessible with numerical relativity simulations. In future work, we plan to explore the parameter space of long-evolved magnetised circumbinary discs, in order to search for characteristic features that could suggest EM signatures.

*Acknowledgements.* We thank the anonymous referee for very useful comments that improved the quality of the manuscript. We thank Daniel Price and Enrico Ragusa for useful discussions. AL acknowledges support from PRIN MUR '2022935STW'. GF thanks Sormani Mattia Carlo and Zoltán Haiman for their fruitful suggestions on the angular momentum transport interpretation. MB acknowledges support from the Italian Ministry for Universities and Research (MUR) programme 'Dipartimenti di Eccellenza 2023–2027', within the framework of the activities of the Centro Bicocca di Cosmologia Quantitativa (BiCoQ). AF acknowledges financial support from the Unione europea – Next Generation EU, Missione 4 Componente 1 CUP G43C24002290001.

## References

- Agazie, G., Anumarlapudi, A., Archibald, A. M., et al. 2023, *ApJ*, **951**, L8  
Amaro-Seoane, P., Aoudia, S., Babak, S., et al. 2012, *ArXiv e-prints* [arXiv:1201.3621]  
Amaro-Seoane, P., Audley, H., Babak, S., et al. 2017, *ArXiv e-prints* [arXiv:1702.00786]  
Avara, M. J., Krolik, J. H., Campanelli, M., et al. 2024, *ApJ*, **974**, 242  
Blanchet, L. 2014, *Liv. Rev. Relat.*, **17**, 2  
Bode, T., Haas, R., Bogdanović, T., Laguna, P., & Shoemaker, D. 2010, *ApJ*, **715**, 1117  
Bogdanović, T., Bode, T., Haas, R., Laguna, P., & Shoemaker, D. 2011, *Class. Quant. Grav.*, **28**, 094020  
Bogdanović, T., Miller, M. C., & Blecha, L. 2022, *Liv. Rev. Relat.*, **25**, 3  
Bowen, D. B., Mewes, V., Campanelli, M., et al. 2018, *ApJ*, **853**, L17  
Bright, J. C., & Paschalidis, V. 2023, *MNRAS*, **520**, 392  
Capelo, P. R., Volonteri, M., Dotti, M., et al. 2015, *MNRAS*, **447**, 2123  
Cattorini, F., & Giacomazzo, B. 2024, *Astropart. Phys.*, **154**, 102892  
Cattorini, F., Giacomazzo, B., Haardt, F., & Colpi, M. 2021, *Phys. Rev. D*, **103**, 103022  
Cattorini, F., Maggioni, S., Giacomazzo, B., et al. 2022, *ApJ*, **930**, L1  
Chang, E., & Youdin, A. N. 2024, *ApJ*, **976**, 100  
Chiesa, A., Izquierdo-Villalba, D., Sesana, A., et al. 2025, *A&A*, **707**, A89  
Cocchiararo, F., Franchini, A., Lupi, A., & Sesana, A. 2024, *A&A*, **691**, A250  
Cocchiararo, F., Franchini, A., Lupi, A., & Sesana, A. 2025, *ArXiv e-prints* [arXiv:2510.21919]  
Combi, L., & Ressler, S. 2024, <https://doi.org/10.5281/zenodo.10841021>  
Combi, L., & Ressler, S. M. 2026, *Phys. Rev. D*, **113**, 044023  
Combi, L., Lopez Armengol, F. G., Campanelli, M., et al. 2021, *Phys. Rev. D*, **104**, 044041  
Combi, L., Lopez Armengol, F. G., Campanelli, M., et al. 2022, *ApJ*, **928**, 187  
Cszmadia, P., Debreczeni, G., Rácz, I., & Vasúth, M. 2012, *Class. Quant. Grav.*, **29**, 245002  
d'Ascoli, S., Noble, S. C., Bowen, D. B., et al. 2018, *ApJ*, **865**, 140  
Dotti, M., Colpi, M., & Haardt, F. 2006, *MNRAS*, **367**, 103  
Dotti, M., Sesana, A., & Decarli, R. 2012, *Adv. Astron.*, **2012**, 1  
Dotti, M., Bonetti, M., Rigamonti, F., et al. 2023, *MNRAS*, **518**, 4172  
Duffell, P. C., Dittmann, A. J., D'Orazio, D. J., et al. 2024, *ApJ*, **970**, 156  
Eggleton, P. P. 1983, *ApJ*, **268**, 368  
Ennoggi, L., Campanelli, M., Zlochower, Y., et al. 2025a, *Phys. Rev. D*, **112**, 063009  
Ennoggi, L., Campanelli, M., Krolik, J., et al. 2025b, *ArXiv e-prints* [arXiv:2509.10319]  
EPTA Collaboration, InPTA Collaboration, Antoniadis, J., et al. 2023, *A&A*, **678**, A50  
Fedrigo, G., & Lupi, A. 2025, *A&A*, **700**, A112  
Fedrigo, G., Cattorini, F., Giacomazzo, B., & Colpi, M. 2024, *Phys. Rev. D*, **109**, 103024  
Franchini, A., Sesana, A., & Dotti, M. 2021, *MNRAS*, **507**, 1458  
Franchini, A., Lupi, A., & Sesana, A. 2022, *ApJ*, **929**, L13  
Franchini, A., Lupi, A., Sesana, A., & Haiman, Z. 2023, *MNRAS*, **522**, 1569  
Franchini, A., Bonetti, M., Lupi, A., & Sesana, A. 2024a, *A&A*, **686**, A288  
Franchini, A., Prato, A., Longarini, C., & Sesana, A. 2024b, *A&A*, **688**, A174  
Giacomazzo, B., Baker, J. G., Miller, M. C., Reynolds, C. S., & van Meter, J. R. 2012, *ApJ*, **752**, L15  
Gold, R. 2019, *Galaxies*, **7**, 63  
Gold, R., Paschalidis, V., Etienne, Z. B., Shapiro, S. L., & Pfeiffer, H. P. 2014, *Phys. Rev. D*, **89**, 064060  
Gutiérrez, E. M., Combi, L., Noble, S. C., et al. 2022, *ApJ*, **928**, 137  
Hénon, M. 1965, *Ann. Astrophys.*, **28**, 992  
Hopkins, P. F. 2015, *MNRAS*, **450**, 53  
Kaaz, N., Liska, M., Tchekhovskoy, A., Hopkins, P. F., & Jacquemin-Ide, J. 2025, *ApJ*, **979**, 248  
Kocsis, B., Frei, Z., Haiman, Z., & Menou, K. 2006, *ApJ*, **637**, 27  
Krauth, L. M., Davelaar, J., Haiman, Z., et al. 2023, *MNRAS*, **526**, 5441  
Leahy, D. A., & Leahy, J. C. 2015, *Comput. Astrophys. Cosmol.*, **2**, 4  
Lopez Armengol, F. G., Combi, L., Campanelli, M., et al. 2021, *ApJ*, **913**, 16  
Lovelace, R. V. E., Li, H., Colgate, S. A., & Nelson, A. F. 1999, *ApJ*, **513**, 805  
Lupi, A. 2023, *MNRAS*, **519**, 1115  
MacFadyen, A. I., & Milosavljević, M. 2008, *ApJ*, **672**, 83  
Manikantan, V., Paschalidis, V., & Bozzola, G. 2025, *ApJ*, **984**, L47  
Mayer, L., Kazantzidis, S., Mastropietro, C., & Wadsley, J. 2007, *Nature*, **445**, 738  
Mignon-Risse, R., Varniere, P., & Casse, F. 2023, *MNRAS*, **520**, 1285  
Mignon-Risse, R., Varniere, P., & Casse, F. 2025, *MNRAS*, **544**, 4226  
Muñoz, D. J., Lai, D., Kratter, K., & Miranda, R. 2020, *ApJ*, **889**, 114  
Noble, S. C., Mundim, B. C., Nakano, H., et al. 2012, *ApJ*, **755**, 51  
Noble, S. C., Krolik, J. H., Campanelli, M., et al. 2021, *ApJ*, **922**, 175  
Paczynski, B. 1977, *ApJ*, **216**, 822  
Paczynski, B., & Wiita, P. J. 1980, *A&A*, **88**, 23  
Paschalidis, V., Bright, J., Ruiz, M., & Gold, R. 2021, *ApJ*, **910**, L26  
Price, D. J., Wurster, J., Nixon, C., et al. 2017, *Astrophysics Source Code Library* [record ascl:1709.002]  
Reardon, D. J., Zic, A., Shannon, R. M., et al. 2023, *ApJ*, **951**, L6  
Rigamonti, F., Severgnini, P., Sottocorno, E., et al. 2025, *A&A*, **693**, A117  
Rudak, B., & Paczynski, B. 1981, *Acta Astron.*, **31**, 13  
Ruiz, M., Tsokaros, A., & Shapiro, S. L. 2023, *Phys. Rev. D*, **108**, 124043  
Shakura, N. I., & Sunyaev, R. A. 1973, *A&A*, **24**, 337  
Shi, J., Krolik, J. H., Lubow, S. H., & Hawley, J. F. 2012, *ApJ*, **749**, 118  
Xu, H., Chen, S., Guo, Y., et al. 2023, *RAA*, **23**, 075024